J. Materials, Conc. Struct., Pavements, JSCE, No. 557/V-34, 135-144, 1997 February

INVESTIGATION OF MODE-I FRACTURE OF EARLY AGE CONCRETE BY A NON-LOCAL PLASTICITY APPROACH

Khan Mahmud AMANAT[1] and Tada-aki TANABE[2]

[1]Member of JSCE, Graduate student, Dept. of Civil Eng., Nagoya University, Japan (1 Furo-cho, Chikusa-ku, Nagoya 464-01)
[2]Member of JSCE, Professor, Dept. of Civil Eng., Nagoya University, Japan (1 Furo-cho, Chikusa-ku, Nagoya 464-01)

An analysis is made to study the fracture and strain localization process of concrete at early age based on the tension experiment[1] made previously. Based on the experiment a tensile softening rule is proposed for concrete at early age. Then a numerical study was made using the non-local gradient-plasticity approach[2] to simulate the evolution of the localized fracture process. It has been shown that the proposed softening rule can be successfully applied to simulate the fracture of early age concrete within the framework of non-local gradient dependent continuum plasticity approach and enables us to describe the early age fracture of concrete in an analytical framework.

Key Words: *concrete, fracture, localization, early age, plasticity, gradient plasticity*

1. INTRODUCTION

Current design practices to control cracks in massive concrete structures are still based on strength criteria[3] rather than on fracture mechanics based criteria. Recent study[4] shows that the strength criteria is not fully valid for large scale structures and the size of the structure itself plays an important role on the load carrying capacity of the structure. Such problems are clearly identified in fracture mechanics[4]. It has been shown that fracture mechanics based design is more realistic for massive or large concrete structures where size effect significantly influences the design. However, application of fracture mechanics in design of concrete structures requires the knowledge of fracture energy consumed by concrete while cracking due to different kinds of loading. Unlike ordinary concrete structure, massive concrete requires some additional design consideration resulting from the need to control cracks at early age due to the differential thermal strain produced by the heat of hydration. Due to the low conductivity of concrete the heat generated by the cement hydration process cannot be dissipated quickly and produces thermal stress that eventually leads to premature cracks in the structure even before any external load is applied. Although such cracks may not be harmful to the loading capacity, these cracks can severely affect the durability and serviceability of the structures. For the reason mentioned above, design to control such cracks require the knowledge of various physical properties as well as the fracture energy consumed by concrete at early ages. Recently a number of researchers[5),6),7),8),9)] addressed this problem and gave effort to understand various chemical, physical and mechanical properties of cement and concrete at early ages. However, it appears that the fracture process of concrete at early age is still one of the least understood aspect of concrete. Fracture of concrete is a highly localized phenomena where failure is induced by concrete cracking principally in mode-I type crack and the post-peak load response decreases sharply with increasing deformation. Study[10)] shows that in the fracture process zone stress does not drop suddenly, instead, it follows a progressive strain softening due to non-homogeneous deformations resulting from macroscopic cracking[11)]. It shows some ductility, because the faces of cracks are connected by grain bridges which delay crack propagation and opening[11)].

Recognizing the strain softening characteristics of the fracture process of concrete it is possible to simulate the same in the domain of continuum

mechanics. Application of classical plasticity can be applied but it has a few major drawbacks - the result is mesh sensitive, fracture process zone cannot propagate beyond those area defined explicitly beforehand, strain field between the boundary of fracture process zone and elastic zone is discontinuous, and the ellipticity of the governing differential equation is lost in the post peak regime. These drawbacks can be overcome by the use of enhanced continuum approaches like the integral approach[12] or gradient plasticity approach[2),13),14),15)]. In this study the gradient approach has been adopted to simulate the fracture process of early age concrete. The essence of this approach is to make the strength degradation dependent on the Laplacian of damage.

An experimental study was made by Lokuliyana[1)] on early age concrete to study the fracture characteristics of concrete. He also made an analytical study based on classical plasticity approach. In this study the same test results were used to verify the analytical study and a comparison is also presented. To simulate the post peak response a strain softening rule is proposed and it was shown that it can successfully describe the fracture behavior of concrete at early age.

2. FIELD EQUATIONS AND FINITE ELEMENT APPROACH

It appears that the integral approach of strain localization problems is only effective for certain kind of total stress strain relationships and its incremental approach is difficult or impossible to implement and its finite element implementation is somewhat awkward. On the other hand gradient plasticity approach has a very sound mathematical base. Due to the descretezation of plastic multiplier along with the displacement field it becomes quite a routine matter to implement gradient plasticity approach in an incremental finite element algorithm. Here a brief description of the field equations of gradient plasticity[2)] is presented. First we consider the following set of field equations:

$$\mathbf{L}^{\mathrm{T}}\dot{\sigma} = 0 \tag{1}$$

$$\dot{\varepsilon} = \mathbf{L}\dot{\mathbf{u}} \tag{2}$$

$$\dot{\sigma} = \mathbf{D}\left(\dot{\varepsilon} - \dot{\lambda}\frac{\partial f}{\partial \sigma}\right), \qquad \dot{\lambda} \geq 0, \tag{3}$$

$$f\left(\sigma, \kappa, \nabla^2\kappa\right) = 0 \tag{4}$$

In the preceding equations $\mathbf{L}$ is a differential operator matrix, $\dot{\sigma}$ and $\dot{\varepsilon}$ are the stress and strain rate tensors respectively, $\dot{\mathbf{u}}$ is a displacement rate vector, $\mathbf{D}$ is the elastic stiffness matrix, λ is a multiplier being a measure of inelastic flow intensity, f is the gradient dependent failure surface and κ is an invariant measure of fracture strain or damage. In the gradient plasticity formulation it is assumed that $\dot{\kappa} = \eta\dot{\lambda}$ where η is a positive constant. With classical strain hardening approach and the failure function considered in this study the value of η becomes unity.

The gradient dependence of the failure function makes the fracture flow consistency condition $df=0$ to become a differential equation with second order spatial gradient terms,

$$\mathbf{n}^{\mathrm{T}}\dot{\sigma} - h\dot{\lambda} + g\nabla^2\dot{\lambda} = 0 \tag{5}$$

with the notations,

$$\mathbf{n} = \frac{\partial f}{\partial \sigma}, \; h = \frac{\partial f}{\partial \kappa}, \; g = \eta\frac{\partial f}{\partial \nabla^2\kappa} \tag{6}$$

Here h is the softening parameter and g is the gradient influence factor. If $g=0$ then equation (5) reduces to classical plasticity equation. Due to the presence of $\nabla^2\lambda$ a direct solution for λ from equation (5) is not possible in general. Therefore, the inelastic strains are discretized using the same mesh of the finite elements as used for the discretization of displacements. For finite element formulation an incremental-iterative algorithm is presented by de Borst[2)], which requires a weak satisfaction of the equilibrium condition (equation 1) and the failure condition (equation 4) at the end of iteration $j+1$ of the current loading step, which results in the following two variational equations

$$\int_V \delta\varepsilon^{\mathrm{T}}\mathbf{D}\left(\mathrm{d}\varepsilon - \mathrm{d}\lambda\mathbf{n}\right)\mathrm{d}V = \int_S \delta\mathbf{u}^{\mathrm{T}}\mathbf{t}_{j+1}\mathrm{d}V - \int_V \delta\varepsilon^{\mathrm{T}}\sigma_j\mathrm{d}V \tag{7}$$

and,

$$\int_V \delta\lambda\left[\mathbf{n}^{\mathrm{T}}\mathbf{D}\mathrm{d}\varepsilon - \left(h + \mathbf{n}^{\mathrm{T}}\mathbf{D}\mathbf{n}\right)\mathrm{d}\lambda + g\nabla^2(\mathrm{d}\lambda)\right]\mathrm{d}V = -\int_V \delta\lambda f\left(\sigma_j, \kappa_j, \nabla^2\kappa_j\right)\mathrm{d}V \tag{8}$$

In the preceding equations d indicate an increment. In equations (7) and (8) only first derivative of $\mathbf{u}$ appears whereas for λ second derivatives appear. Therefore $\mathbf{u}$ is discretized using quadratic C^0 shape functions $\mathbf{N}$ and λ is discretized using Hermitian cubic C^1 shape functions $\mathbf{h}$.

$$\mathbf{u} = \mathbf{N}\mathbf{a}, \qquad \lambda = \mathbf{h}^{\mathrm{T}}\Lambda \tag{9}$$

where **a** is nodal displacement vector and Λ is a vector of nodal degrees of freedom for λ. Using a strain nodal displacement matrix $\mathbf{B} = \mathbf{LN}$ and a vector **p** containing Laplacians of the shape functions **h** we obtain from equation (9),

$$\varepsilon = \mathbf{Ba}, \qquad \nabla^2\lambda = \mathbf{p}^{\mathrm{T}}\Lambda \tag{10}$$

Substituting identities (9) and (10) in equations (7) and (8) and requiring that these equations hold true for any admissible value of $\delta\mathbf{a}$ and $\delta\Lambda$, we obtain the following set of matrix equation,

$$\begin{bmatrix} \mathbf{K}_{aa} & \mathbf{K}_{\lambda a}^{\mathrm{T}} \\ \mathbf{K}_{\lambda a} & \mathbf{K}_{\lambda\lambda} \end{bmatrix} \begin{bmatrix} \mathrm{d}\mathbf{a} \\ \mathrm{d}\Lambda \end{bmatrix} = \begin{bmatrix} \mathbf{f}_e + \mathbf{f}_a \\ \mathbf{f}_\lambda \end{bmatrix} \tag{11}$$

where $\mathbf{K}_{aa}$ is the elastic stiffness matrix, $\mathbf{f}_e$ is the external force vector and $\mathbf{f}_a$ is the nodal forces equivalent to internal stresses defined conventionally. The off-diagonal matrix $\mathbf{K}_{\lambda a}$ and the gradient dependent matrix $\mathbf{K}_{\lambda\lambda}$ are defined as,

$$\mathbf{K}_{\lambda a} = \int_V \mathbf{h}\mathbf{n}^{\mathrm{T}}\mathbf{D}\mathbf{B}\mathrm{d}V \tag{12}$$

$$\mathbf{K}_{\lambda\lambda} = \int_V \left[\left(h + \mathbf{n}^{\mathrm{T}}\mathbf{D}\mathbf{n}\right)\mathbf{h}\mathbf{h}^{\mathrm{T}} - g\mathbf{h}\mathbf{p}^{\mathrm{T}}\right]\mathrm{d}V \tag{13}$$

and the vector of residual forces $\mathbf{f}_\lambda$ due to inexact fulfillment of the fracture condition reads,

$$\mathbf{f}_\lambda = \int_V f\left(\sigma_j, \kappa_j, \nabla^2\kappa_j\right)\mathbf{h}\mathrm{d}V \tag{14}$$

3. MATERIAL MODEL

In this study we are dealing with mode-I fracture problem of concrete specimen under uniaxial loading. So the simple Rankine maximum principal stress failure criterion is adopted as a condition of continuum fracture. The failure surface is of the form,

$$f\left(\sigma, \kappa, \nabla^2\kappa\right) = \sigma_m - \bar{\sigma}_g\left(\kappa, \nabla^2\kappa\right) \tag{15}$$

where σ_m is the maximum principal stress,

$$\sigma_m = \frac{1}{2}\left(\sigma_x + \sigma_y\right) + \frac{1}{2}\sqrt{\left(\sigma_x + \sigma_y\right)^2 + 4\tau_{xy}^2} \tag{16}$$

and $\bar{\sigma}_g$ is the yield strength which depends on both κ and $\nabla^2\kappa$. In $(\sigma_x, \sigma_y, \tau_{xy})$ stress space Rankine failure function possesses a vertex at $(\bar{\sigma}, \bar{\sigma}, 0)$ point. The existence of this vertex poses some difficulties in return mapping algorithm. In classical plasticity approach this difficulty can be overcome by assuming each smooth part of the failure function as a separate function and then applying Koiter's generalizations. In gradient plasticity this approach is not suitable because λ is also a global variable like the displacement field. An alternate approach is to smoothen the failure function in the vertex regime[15]. In this approach the Rankine square shaped failure surface in tension-tension regime is replaced by a smooth circular one. When this is done, the failure function takes the form,

$$f = \sqrt{\left(\sigma_1^2 + \sigma_2^2\right)} - \bar{\sigma}_g = \sqrt{\left(\sigma_x^2 + \sigma_y^2 + \tau_{xy}^2\right)} - \bar{\sigma}_g = 0 \tag{17}$$

However, an incompatibility exists along the σ_x and σ_y axis in the stress space. Therefore this smoothing approach is will be made active when stress state will be dominated by tension and not by shear. Thus the vertex smoothed failure function can be written as,

$$f = \left(\sigma\mathbf{P}\sigma^{\mathrm{T}}\right)^{1/2} - \bar{\sigma}_g\left(\kappa, \nabla^2\kappa\right) \tag{18}$$

where,

$$\mathbf{P} = \begin{bmatrix} 1 & 0 & 0 \\ 0 & 1 & 0 \\ 0 & 0 & 2 \end{bmatrix}, \quad \sigma = \begin{Bmatrix} \sigma_x \\ \sigma_y \\ \tau_{xy} \end{Bmatrix}$$

From equation (18) the gradient to the yield function takes the form,

$$\mathbf{n} = \frac{\mathbf{P}\sigma}{\left(\sigma^{\mathrm{T}}\mathbf{P}\sigma\right)^{1/2}} \tag{19}$$

The form of $\bar{\sigma}_g$ adopted in this paper is,

$$\bar{\sigma}_g = \bar{\sigma}_t(\kappa) - g(\kappa)\nabla^2(\kappa) \tag{20}$$

where $\bar{\sigma}_t(\kappa)$ is a given standard softening rule and $g(\kappa)$ is a given gradient influence function. For the purpose of studying the behavior of concrete at early age a softening function is proposed. The proposed softening rule is as follows (see **Fig.1**),

$$\bar{\sigma}_t(\kappa) = \frac{f_t}{c_1 + 1}\left[c_1 e^{-c_2\kappa/\kappa_u} + \left(1 - \frac{\kappa}{\kappa_u}\right)\right] \tag{21}$$

Here f_t is the tensile strength, κ_u is the ultimate value of equivalent fracture strain measure, c_1 and c_2 are material parameters. The shape of the softening rule can be adjusted using different values of these parameters. The equation of the softening rule is such that initially the strength will degrade

Table 1 Different forms of $g(\kappa)$

Type	Description		Figure
g1	*Constant:*	$g(\kappa) = l^2 \frac{f_t}{\kappa_u}$	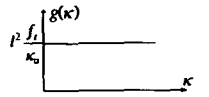
g2	*Linearly decreasing:*	$g(\kappa) = c_3 f_t l^2 \left(1 - \frac{\kappa}{\kappa_u}\right)$ c_3=2500	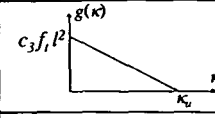
g3	*Non-linear:*	$g(\kappa) = c_4 f_t e^{-c_5 \kappa}$ c_4=35000, c_5=2500	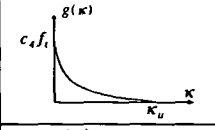
g4	*Proportional to* $\overline{\sigma}_t'(\kappa)$*:*	$g(\kappa) = \frac{f_t l^2}{c_1 + 1}\left(c_1 c_2 e^{-c_2 \frac{\kappa}{\kappa_u}} + \frac{1}{\kappa_u}\right)$	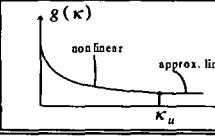

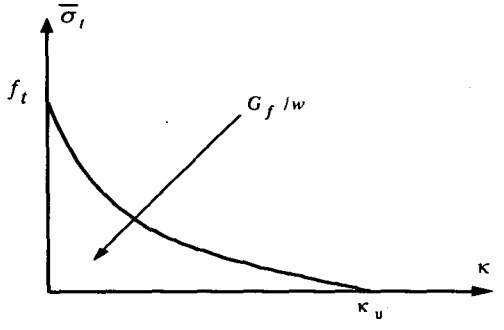

Fig. 1 Softening rule.

exponentially but at later age it will degrade more linearly. This is chosen on the basis of observing the test data on early age concrete. A similar softening rule was proposed for hardened concrete by Hordijk and which was also reported by Pamin[15] which contained similar parameters. Since the change of the properties of fully hardened concrete is very slow, these parameters were taken as constants by Hordijk. For young age concrete this is not true especially at very early ages, since the cement paste in the concrete undergoes hydration process various properties of concrete also change during this process. For this reason it is assumed that the value of c_1 and c_2 will also change with time. The fracture energy is given by,

$$G_f / w \approx \int_0^{\kappa_u} \overline{\sigma}_t(\kappa) d\kappa \qquad (22)$$

where w is the width of the fracture process zone.

Although theoretically it is possible to take any reasonable form of $g(\kappa)$, previous study[16),17)] shows that the form of $g(\kappa)$ plays a significant role in defining the post-peak response. To investigate the effect of $g(\kappa)$ a one dimensional study was made using different forms of $g(\kappa)$ as shown in **Table 1**. For this analysis the l was chosen as 5 mm. Different post-peak responses are given by different forms of $g(\kappa)$ as shown in **Fig.2**. It is seen that although the fracture energy G_f / w is same for the same softening rule (eqn. 21), different forms of $g(\kappa)$ produces different total fracture energy (area under the load-displacement curve). This is due to the fact that the width of the localization zone w is no longer constant. Hence the calculation of G_f according to equation (22) is no longer accurate as long as w is assumed constant and it is mathematically quite formidable to obtain an accurate analytical solution for w when both $g(\kappa)$ and h are varying nonlinearly. For one dimensional case with linear softening rule (h constant) and constant g it was shown[2)] that g and h are related to each other via the internal length scale l as

$$l = \sqrt{-g / h} \qquad (23)$$

In this case the width of the fracture process zone can be calculated exactly as $w = 2\pi l$. **Fig.3** shows the strain distribution obtained for the same one-dimensional analysis. It is clearly seen that different forms of $g(\kappa)$ have effect on both the extension and growth of damage. However, for the last form of $g(\kappa)$, i.e. *g4*, it is observed that the width of the localization zone can be closely approximated as $w \approx 2\pi l$ and also for this type of $g(\kappa)$ both the load-displacement diagram and equation (22) produces approximately same fracture energy G_f. A study in one dimension showed that actually the G_f

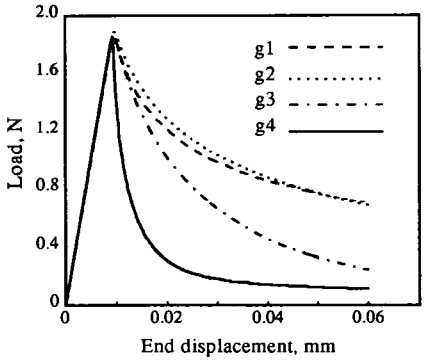

Fig.2 Load displacement response for different forms of $g(\kappa)$.

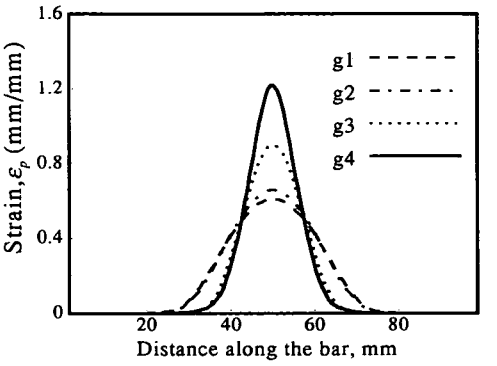

Fig.3 Strain distribution for different forms of $g(\kappa)$.

calculated from eq.(22) overestimates the value by about 10% when it is compared to the energy calculated from the area under the load-displacement response. In this study the last form of $g(\kappa)$ shown in **Table 1** is chosen for analysis. Then by definition of h (equation 6) we can write from equation (20),

$$h = \frac{\partial f}{\partial \kappa} = \eta \frac{\partial \bar{\sigma}_g}{\partial \kappa} = \eta \bar{\sigma}_t'(\kappa) - g'(\kappa)\nabla^2(\kappa) \qquad (25)$$

where prime indicates first derivative with respect to κ and the Laplacian is treated as an independent variable during differentiation and third order terms are neglected.

4. EXPERIMENTAL INVESTIGATION

An experimental study on the fracture process of concrete at early age was performed by Lokuliyana[1] but which is partially reported. Here a brief description follows. The tests were performed on notched prismatic specimens. A sketch of the specimen is shown in **Fig.4**. The dimensions of the specimens are, length = 300mm, width = 140mm and thickness = 40mm. Each specimen was cast with two pieces of steel bars of 18mm diameter at each end to facilitate tensile testing. To force cracks to occur at the middle of the specimen there was a pair of notches at the center of the specimen as shown in **Fig.4**. Each notch had a width of 4.4mm and depth of 25mm and were incorporated in the specimen by inserting two acrylic plates.

Displacement transducer type strain gages were used to measure strain across the notch. For the placement of strain gages, six pairs of small steel studs were placed at front flat face of the specimen at equal intervals as shown in **Fig.5**. Test was carried out for different gage lengths of 20, 30 and 40mm and the studs were placed accordingly. Another two sets of strain gages were placed at the sides of the specimen with a gage length of 50mm to measure longitudinal strain at sides as shown in **Fig.5**.

Tensile strength was calculated by dividing the ultimate load by the cross-sectional area of the specimen at notch. Experimental value of the Young's modulus was calculated from the initial slope of the stress-strain curve. Since there were more than one strain gages, an averaging was done

5. ANALYSIS OF THE TEST RESULTS

For the purpose of computer analysis of the test specimen by finite elements, the test specimen shown in **Fig.4** was descretized using gradient enhanced eight noded plane stress elements. The original specimen was 300mm long with a pair of 18mm diameter steel rods embedded longitudinally at each end of the specimen. The length of the embedded rods were 100mm. Due to the presence of these rods the outer 100mm portions at both end of the specimen were rather stiff compared to the central 100mm portion. This is specially true when we are dealing with young age concrete. At early age both the stiffness and the strength of concrete are very low. So it is quite reasonable to assume that for young age concrete, the two ends having embedded rod elements will behave almost rigidly as compared to the central portion. Based on such assumption when the test specimen was discretized into finite elements, higher stiffness values were assigned to the 100mm portion (portion A and C in **Fig.4**) at the ends. Also another finite element mesh was considered which represented only the central 100mm portion. After making some preliminary analysis, it was observed that both types of mesh discretization give virtually the same result when high stiffness was assigned to the 100mm portions

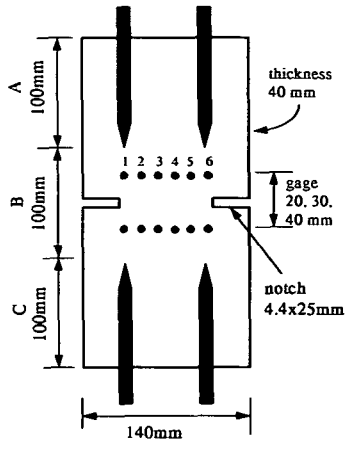

Fig.4 Test specimen

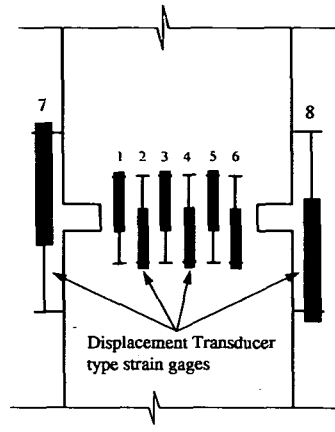

Fig.5 Location of strain gages

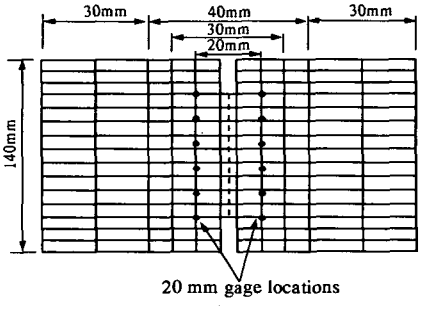

Fig.6 The finite element mesh

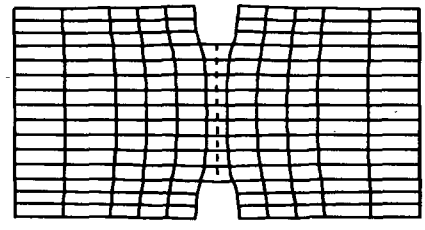

Fig.7 The deformed mesh

at the ends in the former type of mesh. But the second type of mesh was computationally more efficient since it required less number of elements. Hence the later type of discretization was adopted finally for the numerical analysis and the mesh is shown in **Fig.6**. This mesh actually corresponds to 9 hour concrete. For ages 24 hours and higher there was two rows of elements (dotted line in **Fig.6**) at the notch area to cope up with narrower width of fracture process zone. Since the damage is also discretized in gradient plasticity approach, the size of the elements in the potential fractuer zone should be smaller than the anticipated width of the fracture process zone so that damage can propagate over at least two elements.

In the actual test the loading platens were rigid against rotations and during testing the specimen was fixed to the loading platens rigidly. The rigid loading platens and the embedded bars made the setup nearly rigid against any rotation or any lateral deflections. Similar conditions were also applied in the numerical analysis. In the experiment, strains were measured at gage lengths of 20mm, 30mm and 40 mm. And stress was calculated by dividing the load by the cross sectional area at notch. To compare the results of the numerical analysis with the experiment, similar setup was incorporated in the finite element program. For example, strains were calculated from the displacements of nodes 20mm apart to compare the strains measured from 20mm gage length (see **Fig.6**). For the gage locations which do not coincide with element nodes, appropriate interpolation of the displacements of nearby nodes were made.

The original specimen had a pair of notches of dimension 4.4mm x 25mm at midlength. In finite element analysis incorporation of such notches poses some numerical difficulty especially when the notch is narrow and deep. Such meshes are prone to stress locking especially at peak load regime. A remedy is not to include the notch at all and instead incorporate weak elements in the middle. But modeling with notches makes the analysis more realistic and for these reason two 'real' notches were included in the finite element modeling despite the possibility of stress locking phenomenon. In gradient plasticity the problem is more difficult than classical plasticity because of the boundary

Table 2 Values of material parameters

Age	9 hours	16 hours	24 hours	48 hours	72 hours	102 hours
E, MPa	400	1000	6000	8000	11000	14000
ν	0.15	0.15	0.15	0.15	0.15	0.15
c_1	1.0	1.1	1.0	1.0	3.0	1.0
c_2	5.0	5.5	4.0	5.0	5.0	5.0
κ_u	0.009	0.011	0.01	0.009	0.01	0.012
f_t, MPa	0.14	0.25	0.8	1.0	1.25	2.2
l, mm	1.6	2.0	1.0	1.1	1.1	0.8

condition requirement for plastic multiplier λ. In the finite element analysis reduced 2x2 gauss integration was used to calculate the matrices of equation (11) and this required that constraints $\Lambda_n=0$ (Λ_n is the spatial first order dervative of Λ normal to specimen boundary) and $\Lambda_{xy}=0$ (Λ_{xy} is the second order partial spatial derivetive of Λ) to be imposed along the boundary of the whole specimen to make the matrices positive-definite and avoid zero energy modes. Incorporation of such boundary condition at the inside corner makes the structure rather stiff against damage propagation. It was observed that when the value of l is approximately greater than 2 mm or when the value of softening parameter h is too low, such stress locking occurs. In both cases the damage zone tends to propagate far beyond the notch area but the constraints for λ at notch restricts the propagation resulting stress locking and disturbed convergence. Thus, the analysis for 9 hour and 16 hour concrete were more prone to stress locking because of their low tensile strength since low tensile strength results in a lower magnitude of h. However, when the material parameters were adjusted to slightly different values so as to modify the propagation of damage the stress locking phenomenon disappeared.

The values of different material parameters that were taken for the numerical simulations are shown in **Table 2**. The Young's modulus was calculated from the initial slope of the stress strain curve obtained experimentally and an averaging was done over the values calculated from each of the six strain-gages (gages 1 to 6). Due to the lack of experimental data, Poisson's ratio was taken as 0.15. Other values such as κ_u etc. are taken in such a way that the numerical results best fits the experimental data.

6. RESULTS AND DISCUSSION

The results of the finite element analysis are shown in **Fig.8**. This figure shows the comparative aspect of the numerically obtained stress-strain diagram with the experimental ones. Actually there are six strain gages in one specimen and numerically obtained data were tried to fit with all the corresponding experimental results. But due to space limitations only one diagram is shown here for each age of concrete. It should be noted that the experimentally obtained stress strain diagrams for all the strain gages of all specimens were not completely satisfactory. Because it is very difficult to handle the concrete at early ages. In few cases the insertion of the metal studs to fix the strain gages introduced weakness along the gage fixation line and crack occurred at that line instead of occurring at the notch. Such irregular cases are discarded and the rest of the cases where fractures occurred through or near the notched section were considered only.

Fig.8 reveals that in all cases a fairly good agreement between experiment and numerical analysis is obtained. However, it should be noted that these results are obtained using the data shown in **Table 2**. It is possible to alter the values of material parameters and to obtain different results should the experimental stress-strain curves be different. Also it is possible to simulate the same experimental stress-strain data using different combination of material parameters κ_u and l unless we have any data related to the localization process, its width etc. In this study we are dealing with localized fracture. Therefore some pertaining data on localization and fracture must be used to fix a unique set of material parameters. Here it is done by

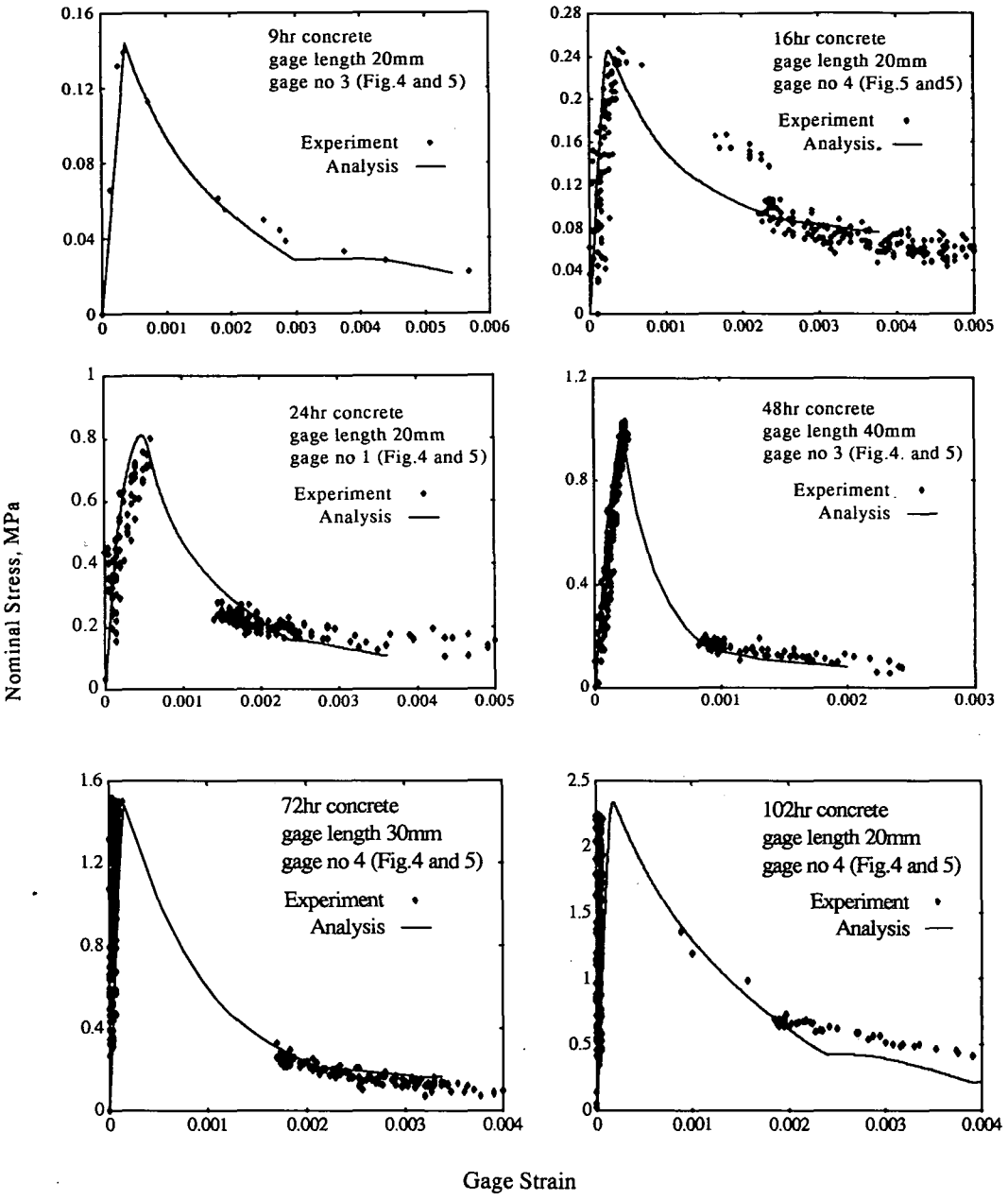

Fig.8 Comparison of numerically and experimentally obtained stress-strain relations

matching the stress strain results obtained for three different gage lengths. Although we do not have any explicit data on width of fracture process zone, the three stress-strain relations corresponding to three different gage lengths comprises a unique set and when numerical results are matched with these, we obtain a unique set of material properties. Here only the result for 72hr concrete is shown in detail (**Fig. 9** and **Fig. 10** in conjunction with bottom left graph of **Fig.8**). The bottom-left graph of **Fig.8** combined with **Fig.9** and **Fig.10** shows fairly good agreement between test and analysis for all three cases of gage length. For brevity results for only one gage lengths in case of other ages are shown in **Fig.8**. A kink in the stress-strain diagram for 9 hour concrete is observed when the strain is about 0.003. Similar case happened for 102 hour concrete also. This is due to the fact that at this point all the gauss integration points (points at which stress, strains, damage etc. are monitored) reach the ultimate value of equivalent fracture strain κ_u. However the value of the gradient influence factor $g(\kappa)$ does not

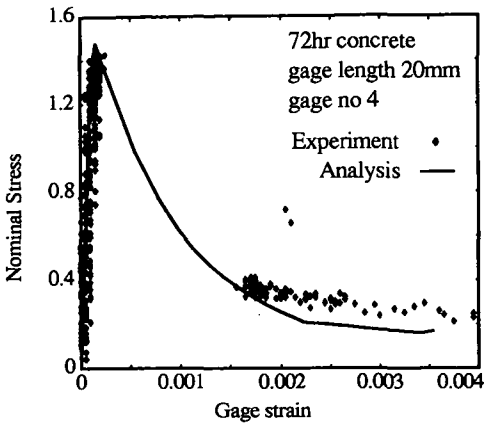

Fig. 9 Stress-strain relationship for 72hr concrete.

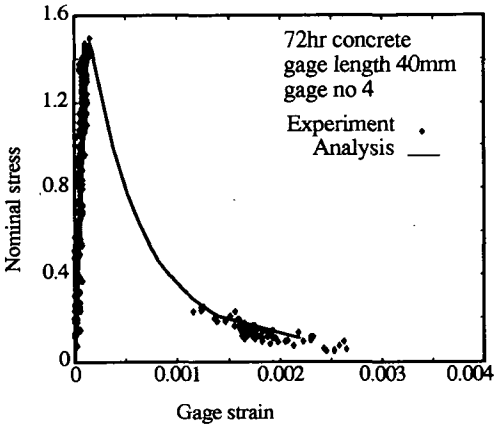

Fig.10 Stress strain relationship for 72hr concrete

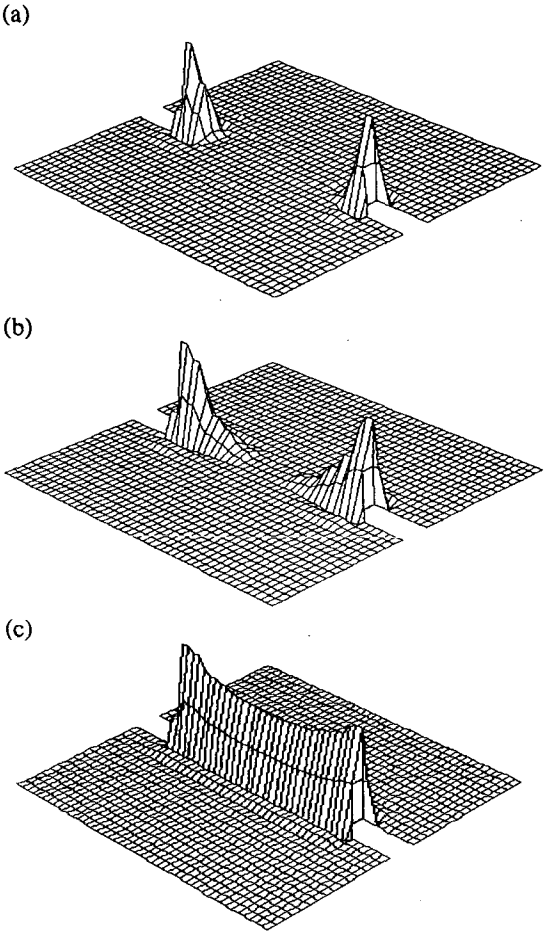

Fig.11 Growth of damage at different loading stages.

become zero at this stage. This is because $g(\kappa)$ is proportional to $\overline{\sigma}_1'(\kappa)$ and $\overline{\sigma}_1'(\kappa_u)$ is not zero when κ reaches κ_u. Due to this reason, the gradient dependent yield strength $\overline{\sigma}_g(\kappa)$ does not reduces to zero. At this stage the value of softening parameter h depends only on $g(\kappa)$ and hence becomes positive at few gauss points in the mostly stressed elements along the notch which is a violation of the gradient plasticity formulation. This phenomena suggests that at or after such loading stage g should also gradually reduce to a considerably smaller value so that such a sharp kink in the numerically obtained stress-strain relation is avoided. But to maintain the non-local nature of the gradient plasticity approach g should not be allowed to become absolutely zero. However, despite such irregularities the overall tangent stiffness matrix remains positive definite and the convergence of the global iterations is not impaired.

The deformed mesh for 48 hour specimen at peak load is shown in **Fig.7** and the progressive growth of damage is shown in **Fig.11** for different loading stages. As expected due to the presence of notch, the outer most elements at notch yield first and gradually the damage grows inwards. **Fig.11a** shows the damage at just after all the gauss points of the outer most elements yielded. **Fig.11b** shows the damage distribution at peak load and **Fig.11c** shows the same at 80% of peak load after the peak. Unlike the classical plasticity approach or the crack-band approach the damage distribution is continuous which is the result of global descretization of plastic multiplier λ in the gradient plasticity approach.

A look at **Table 2** reveals that the value of parameter c_1 at all ages was about 1.0 except for 72 hours. Value of c_2 varies between 4.0 and 5.5. Hence it can be suggested that for early age concrete

considered, c_1 and c_2 can be fixed at values 1.0 and 5.0 respectively. The magnitude of κ_u varied from 0.009 to 0.011 but not in any definite order. On the other hand, internal length scale l varied from 2 mm to 0.8 mm and a trend of decreasing the value of l with age can be observed. l becomes smaller as the concrete gets matured. This is quite logical in the sense that as the concrete gets matured it becomes more brittle and the width of the fracture process zone gets narrower because of the increase in brittleness. l directly governs the width of the fracture process zone w which is approximately given by $w \approx 2\pi l$. However, the relationship of l with age of concrete cannot be linear because in that case l will become zero at some later age. This is not practical because zero l means that the width of the fracture process zone will become zero. To establish a definite relationship of the internal length factor, l, with age or some other material parameters more study, both experimental and numerical, is needed.

7. CONCLUSION

The fracture process of early age concrete was identified through an experimental and analytical study. In the analytical study plastic modeling was done based on non-local gradient plasticity approach. A softening function to describe the fracture process of early age concrete is proposed and it is shown that the softening rule can be applied to simulate the fracture process of early age concrete using the non-local gradient dependent continuum. It has been shown that to fix the appropriate values of material parameters test data on the localization process is necessary in gradient plasticity approach. The results also suggest that the gradient influence factor g needs to be modified at the later stage of loading (when $\kappa \rightarrow \kappa_u$) in order to render more realistic stress-strain relation at higher value of damage and work is in progress in this area. In order to establish some definite relation of some model parameters like l and κ_u with age of concrete or other physical properties of concrete more experimental study is necessary.

REFERENCES

1) Lokuliyana, D.R.: *Fracture Mechanics Based Analysis of Thermal Crack Propagation of Massive Concrete*, PhD Thesis, Dept. of Civil Engineering, Nagoya University, Japan, 1992.
2) Borst R. de, and Mühlhaus H. B.: Gradient-Dependent Plasticity: Formulation and Algorithmic Aspects, *Int. J. Num. Meth. Eng.*, Vol. 35, pp. 521-639, 1992.
3) ACI Committe 207 : Effect of Restraint, Volume Change, and Reinforcement on Cracking of Mass Concrete, *ACI Materials Journal*, Vol.87, No. 3, pp.271-295, 1990.
4) ACI Committe 446, Fracture Mechanics: Fracture Mechanics of Concrete: Concepts, Models and Determination of Material Properties,
5) Oluokun, F.A., Burdette, E.G., Deatherage J.H.: Elastic Modulus, Poisson's Ratio, and Compressive Strength Relationships at Early Ages, *ACI Materials Journal*, Vol. 88, No. 1, pp.3-10, January-February 1991.
6) Zollinger, D.G., Tang, T., Yoo, R.H.: Fracture Toughness of Concrete at Early Ages, *ACI Materials Journal*, Vol. 90, No. 5, pp.463-471, September-October 1993.
7) Cook, W.D., Miao, B., Aïtcin, P., Mitchell, D.: Thermal Stresses in Large High-Strength Concrete Columns, *ACI Materials Journal*, Vol. 89, No. 1, pp.61-68, 1992.
8) Saouma V.E., Broz, J.J., Brühwiler, E., Boggs, H.L.: Effect of Aggregate and Specimen Size on Fracture Properties of Dam Concrete, *ASCE Journal of Materials in Civil Engineering*, Vol. 3, No. 3, pp.204-218, 1991.
9) Guo, C.: Early-Age Behaviour of Portland Cement Paste, *ACI Materials Journal*, Vol. 91, No. 1, pp.13-25, 1994.
10) Read, H.E. and Hegemier, G.A.: Strain Softening of Rock, Soil and Concrete - a Review Article, *Mechnanics of Materials Journal*, Vol. 3, pp.271-294, 1984
11) Mier, J.G.M. van: Mode-I Fracture of Concrete: Discontinuous Crack Growth and Crack Interface Grain Bridging, *Cement and Concrete Research*, Vol. 21, pp.1-15, 1991
12) Bažant, Z.P. and Pijaudier-Cabot, G.: Non-local Continuum Damage, Localization Instability and Convergence, *Journal of Applied Mechanics*, Vol. 55, pp.287-293, 1988.
13) Mühlhaus H. B. and Aifantis E.C.: A Variational Principle for Gradient Plasticity, *Int. J. Solids Structures*, Vol. 28, pp. 845-857, 1991.
14) Borst R. de, Mühlhaus H. B. and Pamin J: A Gradient Continuum Model for Mode-I Fracture in Concrete and Rock, *Fracture Mechanics of Concrete Structures*, Ed Z.P. Bažant, Elsevier, London & New York, 1992, pp. 252-259.
15) Pamin, J.: *Gradient-Dependent Plasticity in Numerical Simulation of Localization Phenomena*, PhD Thesis, Department of Civil Engineering, Delft University of Technology, Netherlands, 1994.
16) Amanat K.M. and Tanabe T: Numerical Study on Fracture Process of Concrete by Gradient Plasticity Models, *Proc. of International Symposium on New Development in Concrete Science and Technology*, Southeast University, Nanjing, China, Sept., 1995.
17) Amanat K.M. and Tanabe T: Applicability of One Dimensional Gradient Plasticity in Identifying Fracture Process of Concrete, *Proc. of JCI*, Vol. 17, 1995.

(Received December 12, 1995)

非局所化塑性モデルによる若材令コンクリートのモードⅠ破壊の解析

Khan Mahmud AMANAT・田辺　忠顕

コンクリート材料特に若材令時のコンクリートを対象として，その歪み局所化現象を解析し，軟化時の歪み分布や応力分布を明らかにした．その際に，古典塑性学と異なって，歪み勾配を破壊関数の中に取り組んだ gradient plasticity モデルを用い，軟化領域の大きさや，勾配を支配するパラメタを同定した．